

# An Optimisation of a Chordwise Slot to Enhance Lateral Flow Control on a UCAV

Usman ALI\*,<sup>1</sup>, Edmund CHADWICK<sup>1</sup>, Oliviu SUGAR-GABOR<sup>1</sup>

\*Corresponding author

<sup>1</sup>University of Salford, School of Science, Engineering and Environment,  
Salford, M5 4WT, United Kingdom,  
u.ali16@salford.ac.uk\*, e.a.chadwick@salford.ac.uk, o.sugar-gabor@salford.ac.uk

DOI: 10.13111/2066-8201.2022.14.4.1

Received: 15 August 2022/ Accepted: 10 October 2022/ Published: December 2022

Copyright © 2022. Published by INCAS. This is an “open access” article under the CC BY-NC-ND license (<http://creativecommons.org/licenses/by-nc-nd/4.0/>)

**Abstract:** *This research aims to optimise a chordwise slot so that lateral flow control of a flying wing configuration can be enhanced. This was achieved by maximising the airflow rate over the trailing edge control surfaces of the wing. A higher rate of airflow over the trailing edge control surfaces will increase the operability of control surfaces, resulting in enhanced lateral control of the air vehicle at medium to high angles of attack. Four variables describing the chordwise slot are identified for numerical optimisation. They are: location, width, length, and angle of trajectory of chordwise slot relative to freestream. The results of the airflow rate for the wing with an optimised chordwise slot are compared with a baseline clean configuration. The flying wing configuration with a chordwise slot has shown a higher mass flow rate over the control surfaces of the wing in comparison to the baseline clean configuration, demonstrating that an optimised chordwise slot can be implemented on a flying wing configuration as it successfully controls the lateral flow by maximising the flow rate over the trailing edge control surfaces.*

**Key Words:** *CFD Optimisation, Flow Control, Flying Wings, UCAV, Unmanned Air Vehicles, Lateral flow*

## 1. INTRODUCTION

The current generation of Unmanned Combat Air Vehicle (UCAV) technology demonstrators employ flying-wing, edge-aligned configuration to reduce their Radar Cross Section (RCS) characteristics. The resulting wing-sweep angles are non-optimal from an aerodynamic point of view for vehicles designed to cruise at high subsonic Mach numbers [1], [2], [3]. The highly-swept leading edges of these configurations promote separated-vortex flows at moderate-to-high incidence angles, enhancing lift generation but resulting in substantially increased lateral flow to the outboard sections of the wing [4], [5], [6], [2], [7], [8], [9], [10]. This lateral flow separation on outboard sections of the configurations is a limiting factor in the ability to exploit the high-lift generated by the leading-edge vortices. Moreover, separated outboard flows under discussion also adversely impact the stability and control of the air vehicle at medium to high angles of attack, and additionally, it generates a nose pitch-up moment as the angle of attack approaches stall [5], [2], [6], [11], [4], [3]. The intensity of this lateral flow to the outer panels of the wing grows in strength with higher angles of attack as is shown in Fig. 1. The Fig. 1 provides an understanding of what happens to separated-vortex flows as the angle of attack is

increased from  $\alpha = 5^\circ$  to  $20^\circ$ . It can be noticed that flow is attached to the surface of the wing when the angle of attack is  $\alpha = 5^\circ$ . However, the intensity of the lateral flow to the outer panels of the wing increases significantly as angle of attack is increased from  $\alpha = 5^\circ$  to  $20^\circ$ .

As a result of this lateral flow to the outer panels of the wing, the lateral control contributed by trailing edge control surfaces becomes severely restricted, as control surfaces operate in a separated flow [9], [8], [2], [6]. Therefore, the high lift generated by the leading-edge vortices cannot be exploited, as the control surfaces become ineffective in producing the control forces required for the lateral control of air vehicle at medium to high angles of attack. In addition to the deterioration in lateral stability, a powerful nose pitch-up moment is experienced by the air vehicle as angle of attack approaches stall [12], [10].

To alleviate these problems, current research has focused on passive flow control techniques such as leading-edge flaps, barriers, canards and fences [13], [10], [12], [14], [15].

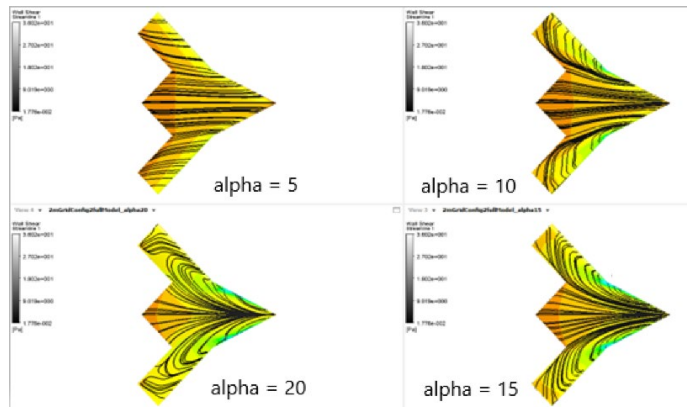


Fig. 1 - Pressure distribution and surface streamlines on upper surface of clean wing for incidence angles from  $\alpha = 5^\circ$  to  $\alpha = 20^\circ$

These flow-control techniques, however, cannot be implemented on the representative flying-wing configuration due to RCS constraints. Leading edge flaps, barriers and vertical fences can have detrimental effects on the RCS signature, hence they must be avoided [1], [2]. The RCS is a measure of how detectable an object is by radar. The main mechanism by which radar signals are returned to the detector is reflection, known as specular return [16], [17]. This occurs when any surface encountered on the aircraft is perpendicular or curved to the radar system. For an air vehicle with perpendicular or curved surfaces, such as vertical fences or leading-edge flaps, the reflections will occur much of the time and the returns will be strong. Vertical aircraft surfaces such as vertical fences or barriers will reflect a large amount of radio signals back to the source. Curved edges should also be avoided as they tend to scatter radar signals [18], [19], [17].

Therefore, as an alternative to the above methods, novel method of chordwise slot is used for the first time on a flying wing configuration and it successfully controls the flow by maximising the lift over control surfaces. The slot under study lies flush with the surface of the wing, and as a result, the effect on RCS signature is expected to be minimal when compared to standard flow-control techniques. Although leading-edge slots have been used on low sweep wings to enhance lift of air vehicles, to the best of authors knowledge they have not been used to maximise the performance of control surfaces on highly swept flying wing configurations. It should be noted that fundamental flow physics of flying wing configurations is different from conventional low sweep wings on which leading-edge slots were previously used. Furthermore, authors have not found any literature on flying wing configurations where

chordwise slots have been used for the purpose of passive flow control. Therefore, this is a novel strand of the research. If slots are permanently open, the extra drag at high speeds is a disadvantage. Therefore, for high speed cruise conditions, slots either can be fitted with a closing valve device [20], or they may be interconnected to control surfaces in such a way that slots open only when control surfaces are deflected. The slots should remain closed when control surfaces are in neutral position [10]. With that said, the slots are easier to construct on a flying wing configuration and are less likely to give operational troubles than movable flaps. Furthermore, they are expected to have a reduced RCS in comparison to leading edge flap as they lie flush with the surface of the wing.

## 2. RESEARCH METHODOLOGY

The investigations on high lift characteristics and lateral flow development over the generic flying wing planform were carried out using a mixture of experimental and computational approaches. The Fig. 2 shows the model considered in this study. The model is a cranked shaped configuration with a leading-edge sweep angle of  $\Lambda = 60^\circ$ , outboard leading-edge sweep of  $\Lambda = 40^\circ$ , trailing edges sweep of  $\Lambda = 40^\circ$  and a root chord length of 0.53m. The model has a thickness of 3mm with sharp edges chamfered at an angle of  $45^\circ$  to promote the formation of separated vortex flows. It should be noted that two types of grids were generated in this study.

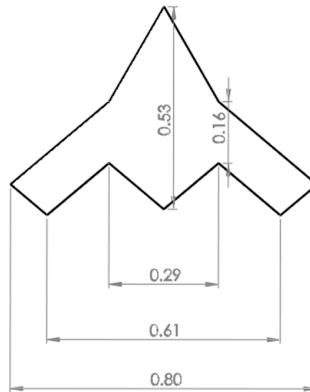


Fig. 2 - Planform view and geometric dimensions of baseline clean configuration

Multiblock structured grids were generated around the baseline clean wings and for the wings with a chordwise slot using ANSA. To determine the operability of trailing edge control surfaces, ICEM was used to generate unstructured grids around wings with deflected control surfaces. The CFD simulations based on Reynolds Averaged Navier-Stokes (RANS) method were computed in Ansys Fluent, and results of predicted simulations were verified with the experiment measured in a wind tunnel.

### 2.1 Experiment Procedure

An experimental investigation was performed on a flat plate UCAV configuration in a low-speed wind tunnel. The model in this study was mounted on a six-component force balance, and in order to have undisturbed upper surface, brackets were mounted on the lower surface of the model using countersink holes as is shown in Fig. 3. The wind tunnel used for the investigations is a low speed closed return tunnel with a test section size of  $0.85\text{m} \times 1.15\text{m}$  (height x width). The freestream velocity of the wind tunnel was adjusted to approximately

32m/s for the investigations in this study. The tunnel has a turbulence intensity of 0.5%, and there is a honeycomb mesh upstream of the settling chamber to reduce transverse turbulence. The freestream conditions are provided by the wind tunnel tests where Mach number was 0.1 and the Reynolds number based on aerodynamic mean chord length was  $5 \times 10^5$ . The test section has a 6-component beam balance with strut mountings to support the models. The reference values for the wind tunnel model are summarised in Table 1. The angle of attack is changed by an interval of  $2.5^\circ$  and the dynamic output for each angle of attack is recorded. The aerodynamic forces and moments were measured as functions of angle of attack in the range of  $\alpha = -10^\circ$  to  $40^\circ$ . When flow conditions in the tunnel have stabilised, the data is collected for a period of 20 seconds and within that time, 100 samples points are recorded by the data acquisition recorder.

**2.2 Computational details of baseline Clean Wing**

The near wall modelling significantly impacts the fidelity of numerical results as solution variables have large gradients in the near-wall region [21]. To achieve good boundary layer resolution, the height of the first cell was placed at  $2.54e^{-6}m$  for RANS computations. This results in  $Y^+$  values of less than 1 for the model, and thus wall function approximations were not used in the solution. To ensure grid independent results, four different grids with increasing number of cells were constructed. The CFD simulations on these four grids were performed at incidence angle of  $29^\circ$  and results were compared with experimental data as is shown in Table 2. It can be seen from Table 2 that successive grid refinements improve the lift and drag coefficients for the wing. The accuracy of the fine grid was examined by performing Richardson extrapolation and calculating the grid convergence index. The mesh of 2 million elements was considered of sufficient accuracy for the problem under study.

For the boundary conditions, no-slip wall was enforced at the surface of the wing, sidewall was set as symmetry and rest of the domain was computed as Riemann Invariants which is called pressure far-field boundary in the Fluent solver. The exterior boundaries were placed at the length of 10 chords from the wing fixed at the centre of symmetry boundary condition.



Fig. 3 - Flat plate flying wing configuration mounted in low-speed wind tunnel

Table 1. - Reference values for the wind tunnel model

Reference Area	0.181136m <sup>2</sup>
Root Chord	0.527701m
Span	0.8m
Mean Aerodynamic Chord	0.37m
Moment Reference Point	0.23m

Table 2. - Comparing grid refinement results for UCAV configuration at incidence angle of 29°

	Nodes of UCAV		Max Y <sup>+</sup>	C <sub>L</sub>	C <sub>D</sub>
	Chordwise	Spanwise			
<b>Number of cells</b>	-	-	-	<b>1.13243</b>	<b>0.75249</b>
<b>0.5m</b>	52	61	0.66	1.06686	0.61261
<b>1m</b>	69	81	0.58	1.09242	0.62653
<b>2m</b>	76	89	0.62	1.11015	0.63146
<b>3m</b>	83	98	0.38	1.12047	0.63725

It should be noted that exterior boundaries with 15 chords length were also tested but there was a negligible difference in the results between the two simulations. Therefore, 10 chords length was chosen for this study. The density-based solver was used for all the simulations in this study and air was computed as an ideal gas. The one equation Spalart-Allmaras turbulence model was used to close the governing equations and the second order upwind scheme was used for the discretisation of the computations. The solution methods in this study are based on implicit scheme with Roe-FDS as flux type, and a higher order accuracy is achieved in Fluent using finite volume formulation. The standard initialisation is computed from far-field boundary condition for all the computations under investigation. The solution of steady state RANS equations is achieved in an iterative manner, and the convergence criteria for all the discretised equations was set to be  $10^{-3}$ . Although, all the computations have achieved minimum convergence criteria of  $10^{-3}$ , but in order to assess the convergence of the solution, aerodynamic forces and moments were monitored for all the computations as the solution progressed to its convergence criteria.

### 2.3 CFD Approach to Optimisation

The objective of this CFD optimisation was to maximise the mass flow rate over the trailing edge control surfaces so that lateral control of the wing can be enhanced at moderate to high angles of attack. The gradient information for the objective function was not available in this study, therefore Pattern Search method was implemented to optimise the chordwise slot under study. The objective function depends on certain input parameters of the problem called variables [22], [23], [24], [25], and the target of the study is to find the values of variables that will maximise the objective function or mass flow rate of the chordwise slot. In the Pattern Search method, independent variables or parameters are changed one at a time to improve the approximation while other variables are held constant [23], [26]. The method finds minimum or maximum of objective function for one variable at a time. In this study, four variables for the chordwise slot were identified which can maximise the objective function over the trailing edge control surfaces of the wing. Those four variables are: location, width, length, and the angle of trajectory of the slot relative to the freestream. The Fig. 4 shows four independent variables that are being optimised in this study. It should be noted that the angle of trajectory of the slot was measured with respect to the trailing edge of the wing as is shown in Fig. 5 (left). The strategy adopted for the optimisation process was to change one parameter at a time to improve the approximation while other parameters were held constant. As only one variable was changed at a time, the problem reduced to a sequence of one-dimensional searches that were solved using the Pattern Search method in conjunction with an interpolation method. The objective function which is mass flow rate for this study was calculated normal to the trailing edge of the wing for each variable. The mass flow rate for each variable, location, width,

length, and angle was calculated by inserting three lines along the trailing edge of the wing as shown in Fig. 5 (right). The three lines were placed at the distance of 2mm, 4mm and 8mm from the surface of the wing, and 30 data points were collected for each line along the trailing edge of the wing.

First location of the slot was determined where maximum flow rate is produced. This was achieved by changing the location of the slot to 8 different positions. Once optimum location of the slot was determined, the width of the slot was varied to 0.5mm, 1mm and 2mm while location of the slot was held constant.

As width of 2mm showed mass flow results similar to 1mm with only a marginal increase for the latter, the slot with 1mm width was chosen for further computations. Similarly, slot length was altered to 0.06m, 0.08m and 0.1m as shown in Fig. 4 (lower left), and CFD computations were carried out to calculate the mass flow rate for each length adjustment. It was established that a slot with the longest length provided the maximum mass flow rate normal to the trailing edge of the wing.

The length of the slot was not increased any further in order to provide sufficient room for the installation of trailing edge control surfaces. Finally, trajectory angle of the slot was varied from  $\theta = 60^\circ$  to  $130^\circ$  with respect to the trailing edge of the wing, while other three optimised variables were held constant. The Fig. 4 (lower right) shows slot angles investigated for the optimisation process. The optimum variables of the slot that were determined after the CFD simulations are summarised in Table 3.

The mass flow rate for each variable, location, width, length, and angle was calculated by inserting three lines along the trailing edge of the wing as shown in Fig. 5 (right). Three lines as opposed to one were used to get better understanding into behaviour of the flow over a bigger region of the trailing edge surface. First, average normal velocity across the lines was calculated using the following relationship:

$$U_n = U \cos\theta + V \sin\theta \quad (1)$$

where  $U_n$  in the above equation is the average normal velocity, and  $\theta$  was calculated to be  $32.7^\circ$  for the wing under study.

The average normal velocity was then converted into mass flow rate by multiplying it with density of air, and the surface area defined by the three lines over the trailing edge of the wing.

An interpolation code was written in Matlab for this optimisation problem to estimate the values between known CFD data points. Matlab function `pchip` was implemented for the interpolation of the data.

If both function values and first derivative is known for a set of data points, then `pchip` interpolation can be used to reproduce the data. The behaviour of `pchip` slope is determined by two data points on either side of a particular interval and the function ignores the points further away [22].

Table 3. - Optimum dimensions of variables for the slot

Variable	Dimension
Location	Location 2
Width	1mm
Length	0.1m
Angle	$130^\circ$

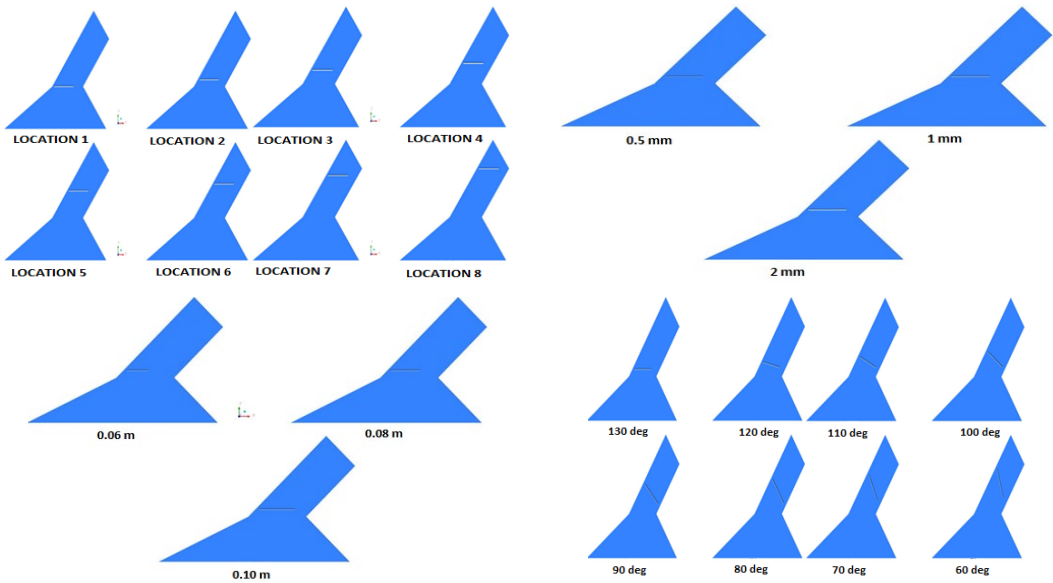


Fig. 4 - The parameters for the optimisation of chordwise slot - Location (upper left); Width (upper right); Length (lower left); Angle (lower right)

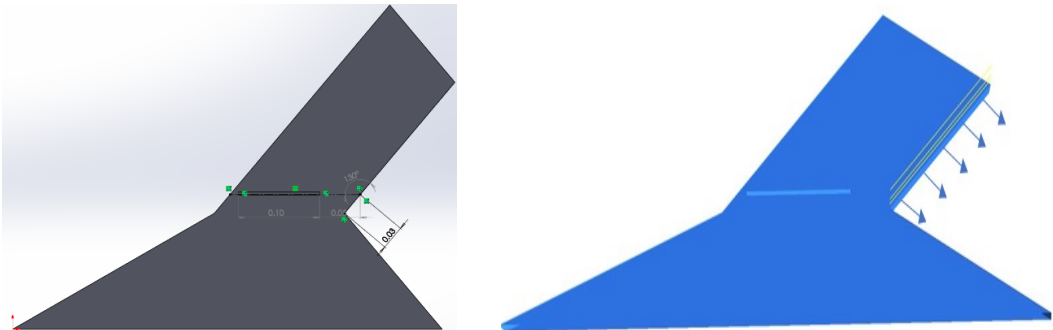


Fig. 5 - Dimensions of optimised chordwise slot (left); horizontal lines on the trailing edge of chordwise slot wing that were used to calculate mass flow rate of the wing (right)

The results of mass flow rate for all four variables with interpolated data points are shown in Fig. 6. The bottom surface of the wing showed negligible difference in mass flow rate between clean wing and wing with a slot.

Therefore, bottom surface was ignored at this stage of the optimisation process. The maximum value of mass flow rate for each variable in interpolated charts was used to design an optimised chordwise slot to control the lateral flow of the wing so that lateral control of the wing can be enhanced.

The authors acknowledge that chordwise slot may pose a structural difficulty for the wing under study, but this area of research can be the subject of a future investigation. As the objective of the current research is to implement a method that can enhance the lateral control of the wing under study, the issue of structural integrity of the wing can itself be the basis of another research topic. With that said, the authors believe that selection of an appropriate material and re-positioning of the spars could overcome the potential structural problems posed by the chordwise slot.

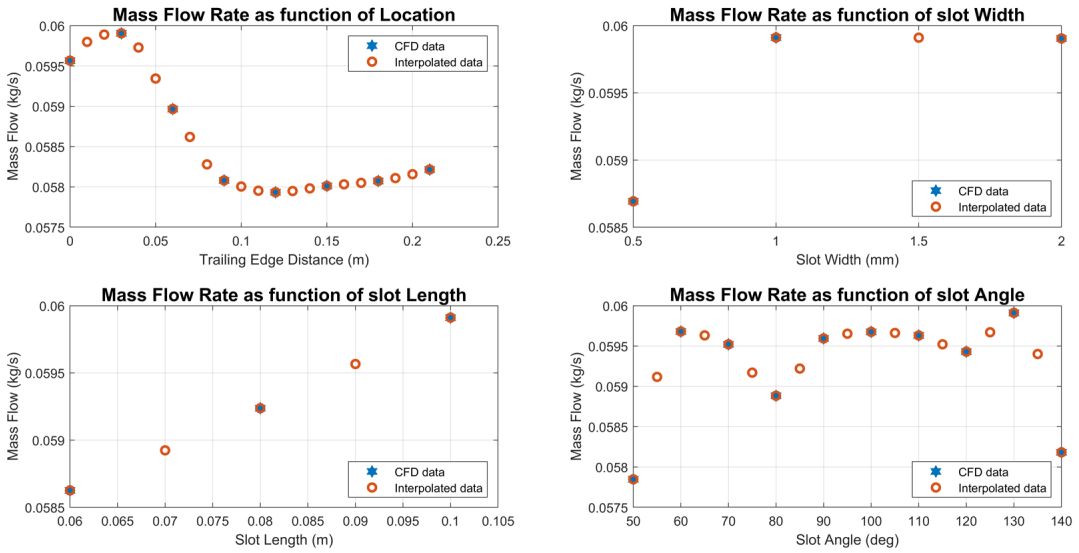


Fig. 6 - Mass flow rate as a function of slot parameters

Table 4 - Mesh parameters for the optimisation study of the wing with and without chordwise slot

Model	Mesh Type	Cells	Growth Ratio
Baseline Clean	Structured	2620144	1.34
Chordwise Slot	Structured	2677550	1.34

Multi-block structured mesh was generated around the baseline clean wing and wing with the chordwise slot. Only half span of models was meshed as symmetric boundary conditions were considered for the wings under study. The grid independence study on a clean wing showed that a grid with 2 million elements can be considered of sufficient accuracy for the problem under investigation. For structured multiblock grids for optimisation study, the height of the first cell normal to the surface of the wing was  $3 \times 10^{-6}$  m, yielding  $Y^+$  values of approximately 1. The grids have a growth rate of 1.34 providing approximately 2.6 million cells as shown in Table 4.

### 2.4 Computational details of wings with deflected Control Surfaces

The results of flow control studies indicated that chordwise slot can be used on the flying wing configuration to limit the intensity of lateral flow to the outboard sections of the wing at moderate to high angles of attack. Therefore, it was important to determine whether chordwise slot in the wing can improve the lift coefficients when trailing edge control surfaces of the wing are deflected. The wing with the higher lift coefficients will provide an enhanced lateral control to the air vehicle at medium to high angles of attack. To achieve this objective, computational analysis was performed on four types of wing designs: clean wing, clean wing with deflected control surface, wing with chordwise slot but zero deflection and lastly wing with chordwise slot and control surface deflection. The Fig. 7 (left) shows the four types of wings used for computational analysis in this study. The control surface for the wings in Fig. 7 is deflected to  $30^\circ$ . The control surface has a cut out of 25% of the local chord. Only half span of the wings is shown in Fig. 7, but full span was computed to predict the lift coefficients of the wings.

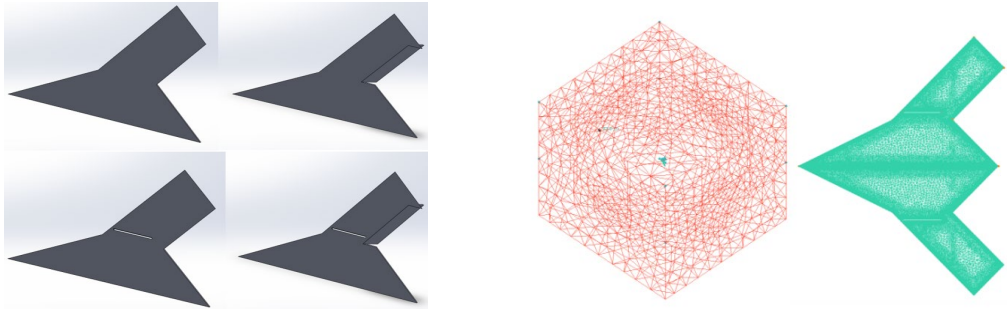


Fig. 7 - Wings used for the calculations of coefficients of lift (left) and topology of unstructured grids (right)

Table 5. - Number of elements used for the computations of the wing

Model	Clean	Clean with Deflected CS	Chordwise Slot	Chordwise Slot with Deflected CS
Elements	2210276	2402778	2155671	2358177

The basic dimensions of the baseline clean wing were provided in earlier part of the paper. For this part of the study, ICEM grid generator was used to construct unstructured grids around clean wings and wings with slots and deflected control surfaces. The wing designs were computed using similar grid sizes as is shown in Table 5. The mesh was mirrored in ICEM to represent the full span of the wings for the calculation of lift coefficients. The boundary conditions and solver settings used for both clean wings and wings with a slot were identical. To capture the effects of viscous boundary layer on the solution, prism mesh was generated near the surface of the wing. The grids have a growth of rate of 1.40 with 20 prismatic layers.

### 3. RESULTS AND DISCUSSIONS

#### 3.1 Flow analysis of baseline clean wings

The predicted coefficients of lift, drag and pitching moments of the configuration in this study are shown in Fig. 8, and results are compared against the data measured in a wind tunnel. The charts of aerodynamic forces and pitching moments show the angles of attack range from  $\alpha = -8^\circ$  to  $40^\circ$ . It can be seen from the Fig. 8 that lift coefficient plot for the configuration show a linear behaviour up to the angles of attack where wing stall occurs. The drop-in lift starts appearing after the stall angles of attack regime, but unlike the deep stall at high Reynolds number as is the case with rectangular and other planform wings, the stall is not abrupt which is the main characteristics of flying-wing configurations [27] [5]. RANS computational method predicts the non-linear part of the lift coefficient well. It can be seen from the moment plots that moment coefficient decreases with an increase in incidence angles without any indication of a significant nose pitch-up behaviour in the incidence range considered. It can also be observed from Fig. 8 that there are differences in drag values at moderate angles of attack, but the overall characteristics of the experiment plot is captured well by the RANS method. The small discrepancy in results between experimental and predicted solutions can possibly be due to the under prediction of vortex strength by the turbulence model. As regions of separated flows become more noticeable at high angles of attack, aerodynamic coefficients and moments become difficult to predict by RANS method with absolute accuracy. With that said, results obtained from a RANS method generally give a similar level of agreement with experiment, but the flow separation and the associated non-linear behaviour appear a little later than in the experiment.

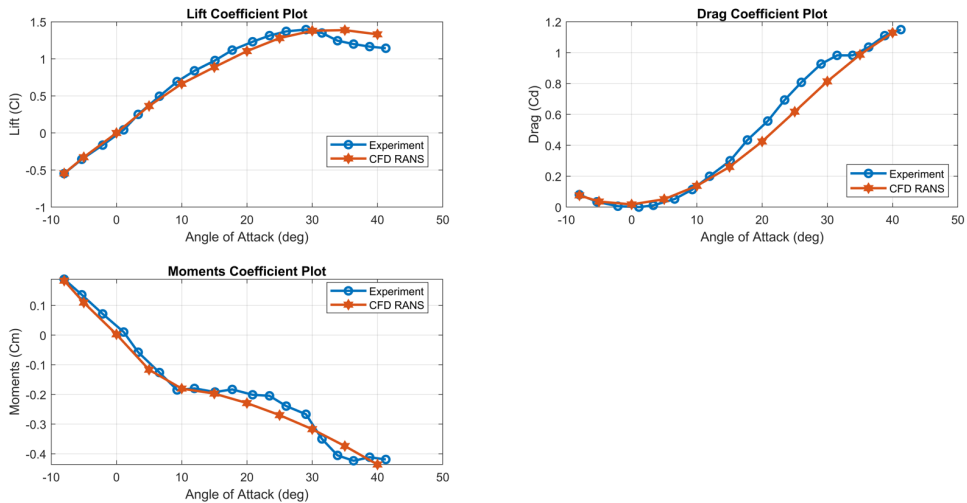


Fig. 8 - Aerodynamic coefficients and pitching moments for the baseline clean UCAV configuration

RANS simulations were performed on baseline clean wing to capture the main characteristic features of the flow. The visualisation of the vortex system on the upper surface of the wing is shown in Fig. 9. It should be noted that results for this plot are calculated for angles of attack ranging from  $\alpha = 5^\circ$  to  $\alpha = 20^\circ$ , and four cross section slices along the wing are positioned at 20%, 40%, 60% and 80% of the chord length. The Fig. 9 shows the slices of pressure coefficient contour on the surface of the wing. This plot enables us to observe the influence of the vortex system on the upper surface of highly swept wing for a range of angles of attack. It can be observed that flow separates from the leading-edge and rolls into two vortex sheets of rotating fluid for the entire range of angles of attack, but the influence of leading-edge vortex is weaker for lower angles of attack. It can be noticed from Fig. 9 that vortices start as small shear layers but grow in size extending from the apex to the trailing edge of the wing. The outer layer increases in diameter with distance from the apex to the trailing edge of the wing. This pair of vortices is the primary cause of high lift and delay in wing stall to higher angles of attack over the highly swept flying wing configurations [27], [5]. A disadvantage, however, is that as the angle of attack is increased these vortices detach from the surface of the wing and experience a lateral flow to the outboard sections of the wing, resulting in loss of lateral control of the wing as trailing edge control surfaces operate in a separated flow condition. The intensity of this lateral flow to the outer panels of the wing grows in strength with the angle of attack making the control of air vehicle difficult as control surfaces become ineffective in producing the control forces required for the lateral stability of the air vehicle at medium to high angles of attack [6], [2]. The lateral control contributed by the trailing edge control surfaces can be enhanced by analysing and controlling the lateral flow development on the suction side of the wing. In CFD absolute helicity is used for the calculation of primary vortex Iso surface. The Fig. 10 shows the plots of absolute helicity-based Iso surface in which phenomenon of vortex breakdown on the surface of the wing can create large changes in pitching moments which can affect the stability of air vehicle [28], [29]. The vortex increases in velocity and energy with the angle of attack, and at low angles of attack the vortex breakdown transpires near the trailing edge of the wing without affecting the vortex lift of the wing. However, at a certain point, a sudden decrease in the strength of the primary vortex occurs [30], [31]. It can be observed from Fig. 10 that vortex breakdown first occurs near the trailing edge of the wing, and then moves forward as the angle

of attack is increased. When vortex breakdown reaches the apex of the wing, a further increase in angle of attack results in loss of coherent vortex flow leading to total flow separation. This can adversely impact the stability and control of the air vehicle at medium to high angles of attack and additionally generate a nose pitch-up moment as the angle of attack approaches stall. Therefore, it is important to control the flow separation of leading-edge vortices so that stability of the air vehicle can be enhanced.

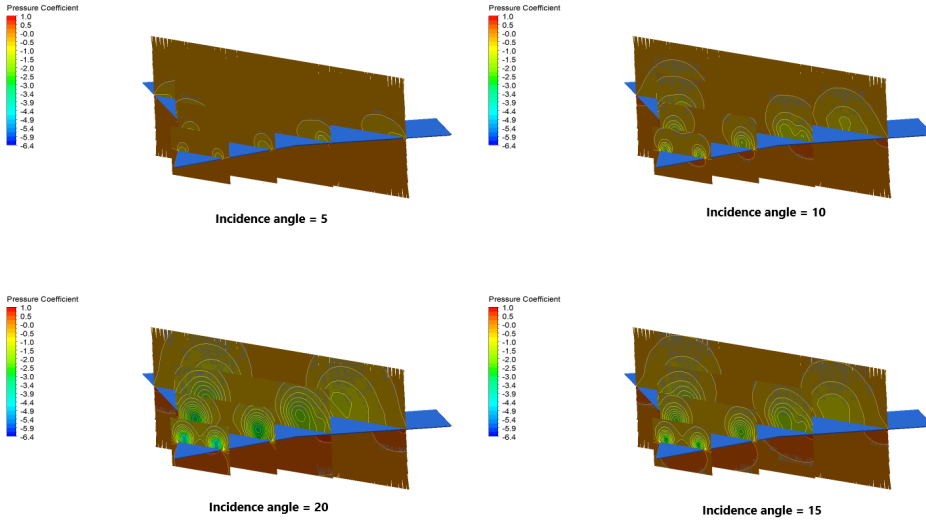


Fig. 9 - Visualisation of the vortex system on the upper surface of clean wing for incidence angles from  $\alpha = 5^\circ$  to  $\alpha = 20^\circ$

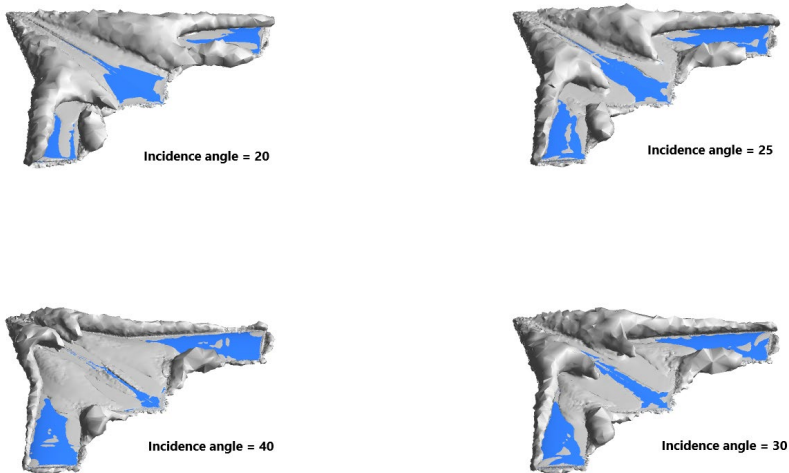


Fig. 10 - Absolute helicity-based Iso surface for incidence angles of  $\alpha = 20^\circ$  to  $\alpha = 40^\circ$

### 3.2 CFD optimisation results

To control the lateral flow development of separated vortex flows on upper surface of the wing at medium to high angles of attack, a novel approach of chordwise slot was implemented on a highly swept flying wing configuration. The Fig. 11 shows pressure distribution and surface streamline comparison between clean wings and wings with chordwise slots at the incidence angles of  $20^\circ$  and  $25^\circ$ . When streamlines are shown together it indicates increased velocity, and when streamlines are wide apart it represents decreased velocity. When streamlines

converge, it means the fluid has accelerated and it has detached from the surface of the wing. On the contrary when they diverge, it indicates decelerating airflow and the associated rise in the pressure [32]. The streamline pattern shows a formation of a vortex behind the chordwise slot of the wing. The vortex stimulates the flowfield of the wing in the opposite direction, and as a result more airflow is routed to the trailing-edge control surfaces of the wing. It can be observed from the streamline pattern that only a small amount of fluid has moved to the outboard sections of the wing, and a considerably higher amount of fluid was routed to the tips of the wing. More airflow towards the tips of the wing will result in more effective control of the spoilers of an air vehicle at medium to high angles of attack. The spoilers are vertical plates that deflect upwards to increase the drag of an air vehicle upon landing [2], [10]. They can also be used to enhance lateral control of the air vehicle.

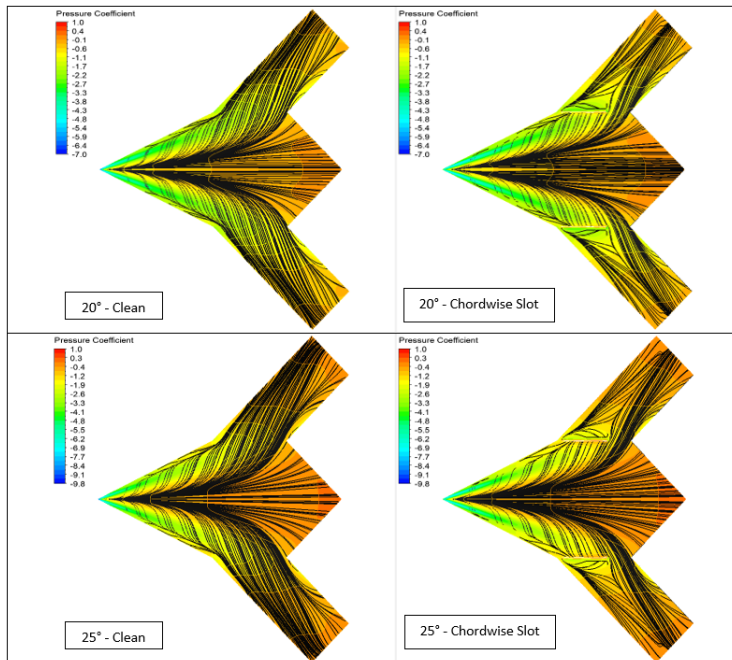


Fig. 11 - Pressure distribution and surface streamlines comparison between clean and chordwise slot models at incidence angles of 20° and 25°

Streamline patterns further illustrate that higher amount of fluid has moved over to the trailing edge control surfaces on wing with the chordwise slot in comparison to the clean wing.

In this study, the focus is on the analysis of medium to high angles of attack for the optimisation problem, as lateral flow on outer sections of flying wing configurations severely affects the manoeuvrability of control surfaces of the vehicle at this range of incidence angles [2] [6]. Although, surface streamlines indicated an improvement in the lateral flow for the wing with the chordwise slot, but it was important to quantify the amount of airflow rate over the trailing edges of the wing. Therefore, the results of mass flow rate on a wing with an optimised chordwise slot were calculated over the trailing edge of the wing and compared against the clean baseline wing as is shown in Fig. 12. It was noticed that there was a negligible difference in mass flow rate on the bottom surface of the wing between clean wing and wing with the slot. However, for accuracy purposes the values of mass flow rate obtained from the bottom surface of the wing were added to the mass flow data of the upper surface of the wings to obtain the total mass flow rate for both clean wing and wing with the slot. Mass flow rate

in this study was measured as functions of angles of attack ranging from  $\alpha = 12.5^\circ$  to  $\alpha = 30^\circ$ . It can be seen in Fig. 12 that there is an increase in mass flow rate for the wing with chordwise slot in comparison to the clean wing. The mass flow rate is consistently higher for the wing with the slot for all angles of attack, ranging from moderate to high angles of attack and then eventually drops down at the incidence angle of  $30^\circ$ . The maximum difference in mass flow rate between clean and wing with the slot was noticed at the incidence angle of  $20^\circ$ . It should be noted that the wing under study stalls at incidence angle of  $30^\circ$  as is shown in Fig. 8. The post stall angles of attack regime is not of interest for the optimisation analysis, as authors are trying to make control surfaces more manoeuvrable only at medium to high angles of attack. The Fig. 12 demonstrate that the chordwise slot method can be implemented on a flying wing configuration as it successfully controls the lateral flow by maximising the flow rate over the trailing edge control surfaces.

It was considered important to determine whether chordwise slot in the wing can improve the lift coefficients at high angles of attack upon the deflection of control surfaces, as the wing with higher lift coefficients will improve the operationality of control surfaces, enhancing the lateral control of the air vehicle.

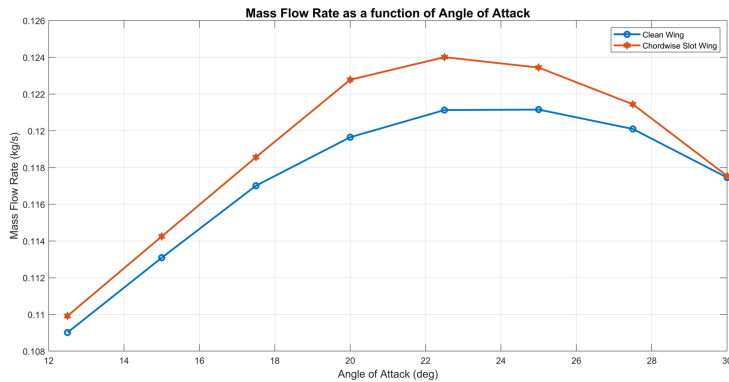


Fig. 12 - Mass flow rate comparison between clean and chordwise slot wing

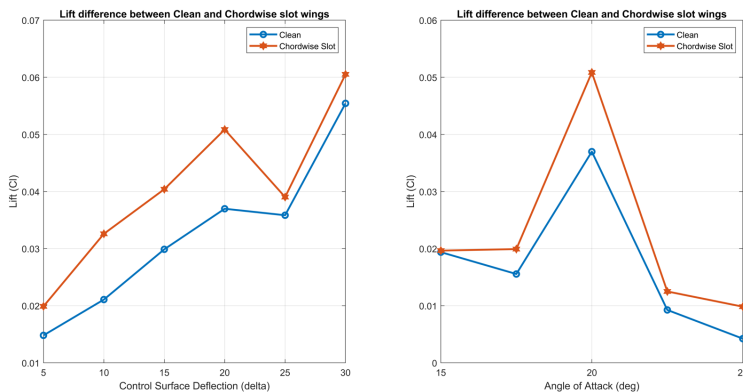


Fig. 13 - Lift difference comparison between wings with and without chordwise slot at constant angle of attack of  $20^\circ$  (left); constant control deflection of  $5^\circ$  (right)

Therefore, CFD investigations were carried out to obtain the change in lift coefficients so that effectiveness of chordwise slots can be quantified. It should be noted that full span of the wings was computed to predict the difference in lift coefficients between clean wings and wings with the chordwise slot. Two sets of CFD analysis were conducted for this purpose. For the first set

of CFD analysis, angle of attack was fixed at  $20^\circ$  while control surface was deflected from  $\delta = 5^\circ$  to  $\delta = 30^\circ$ . For the second set of CFD analysis, angle of attack was changed from  $\alpha = 15^\circ$  to  $\alpha = 25^\circ$  while control surface was fixed at an angle of  $\delta = 5^\circ$ . The left side of Fig. 13 shows the difference in lift coefficients between clean wing and wing with chordwise slot when control surface is deflected in the range of  $\delta = 5^\circ$  to  $30^\circ$ . The right side of Fig. 13 shows the angles of attack range from  $\alpha = 15^\circ$  to  $25^\circ$  with a constant control surface deflection of  $\delta = 5^\circ$ . The lift difference is the increase in lift for the wing when the control surfaces are deflected to the downside. It can be observed from the plots that the change in lift when control surfaces are deflected increases for the wings with the chordwise slot. It can be seen in Fig. 13 that maximum difference in lift occurs at an incidence angle of  $20^\circ$ . It is seen that percentage increase in lift is significant over a range of angles of attack and control surface deflections but the total increase in lift is still small. However, this still demonstrates that the operability of the control surfaces at high angles of attack is improved when the chordwise slot is present.

#### 4. CONCLUSIONS

In this study two main research topics were addressed. The first was to predict and compare high-lift performance of a low observable UCAV configuration using RANS method, and to enhance our understanding of viscous lateral flow development over a highly-swept UCAV configuration. It has been shown that reasonable predictions can be made using RANS as results obtained from the method agree well with the experiment. It was noticed that flow separation and associated non-linear behaviour appear a little later in RANS predictions than in the experiment. The flow physics of viscous lateral flow development and vortex structure were captured well by the RANS method. The vortex system on the upper surface of the wing was visualised with the help of cross section slices for angles of attack ranging from  $\alpha = 5^\circ$  to  $\alpha = 20^\circ$ . The second topic concerned with the optimisation of a chordwise slot to maximise the airflow rate over the trailing edge control surfaces of the flying wing at medium to high angles of attack. For the optimisation of the slot, Pattern Search Method was used by changing four variables of chordwise slot: location, width, length, and angle. The flow control method of a chordwise slot showed that it successfully controls the flow by enhancing the airflow rate over the trailing edge control surfaces of the wing. It was shown that there is an increase in the mass flow rate for the wing with the chordwise slot in comparison to the clean wing. It was important to determine whether chordwise slot in the wing can improve the lift upon the deflection of control surface as the wing with higher lift coefficients will improve the operability of control surfaces enhancing the lateral control of the air vehicle. It was observed that percentage increase in the lift is significant over a range of angles of attack and flap deflections but the total increase in lift is still small. This still demonstrates that the operability of the control surfaces at high angles of attack is improved when chordwise slot is present.

#### REFERENCES

- [1] A. Schütte, D. Hummel, and S.M. Hitzel, Flow Physics Analyses of a Generic Unmanned Combat Aerial Vehicle Configuration, *Journal of Aircraft*, **49**(6): p. 1638-1651, 2012.
- [2] R. H. Barnard, and D. Philpott, *Aircraft flight: a description of the physical principles of aircraft flight*, 2010: Pearson Education.
- [3] I. Gursul, Vortex flows on UAVs: Issues and challenges, *The Aeronautical Journal* (1968), 2004, **108**(1090): p. 597-610.

- [4] J. M. Luckring, The discovery and prediction of vortex flow aerodynamics, *The Aeronautical Journal*, **123**(1264): p. 729-804, 2019.
- [5] S. Gudmundsson, *Chapter 9 - The Anatomy of the Wing*, in *General Aviation Aircraft Design*, S. Gudmundsson, Editor. 2014, Butterworth-Heinemann: Boston, p. 299-399.
- [6] R. S. Shevell, *Fundamentals of Flight*, 2nd ed. 1989, New Jersey: Prentice Hall.
- [7] J. J. Bertin, *Aerodynamics for Engineers*, 4th ed. 2002, USA: Prentice Hall.
- [8] H. Kerstin, S. Andreas, and R. Martin, *Numerical Investigation of the Aerodynamic Properties of a Flying Wing Configuration*, in *30th AIAA Applied Aerodynamics Conference*. 2012, American Institute of Aeronautics and Astronautics.
- [9] N. T. Frink, M. Tormalm, and S. Schmidt, Three Unstructured Computational Fluid Dynamics Studies on Generic Unmanned Combat Aerial Vehicle, *Journal of Aircraft*, **49**(6): p. 1619-1637, 2012.
- [10] A. C. Kermode, *Mechanics of flight*, ed. R.H. Barnard and D.R. Philpott. 2012, New York: Pearson Education.
- [11] N. Robert, et al., *Modification of the Flow Structure over a UAV Wing for Roll Control*, in *45th AIAA Aerospace Sciences Meeting and Exhibit*, 2007, American Institute of Aeronautics and Astronautics.
- [12] S. Gudmundsson, *Chapter 10 - The Anatomy of Lift Enhancement*, in *General Aviation Aircraft Design*, S. Gudmundsson, Editor. 2014, Butterworth-Heinemann: Boston, p. 401-457.
- [13] D. F. Anderson, *Understanding flight*. 2000, New York: McGraw-Hill.
- [14] J. P. Rosenblum, An overview of flow control activities at Dassault Aviation over the last 25 years, *The Aeronautical Journal*, **120**(1225): p. 391-414, 2016.
- [15] P. R. Ashill, J. L. Fulker, and K. C. Hackett, A review of recent developments in flow control, *The Aeronautical Journal* (1968), **109**(1095): p. 205-232, 2005.
- [16] M. Parker, *Chapter 18 - Radar Basics*, in *Digital Signal Processing 101 (Second Edition)*, M. Parker, Editor. 2017, Newnes. p. 231-240.
- [17] E. F. Knott, *Radar cross section measurements*, Raleigh, NC: SciTech Pub, 2006.
- [18] L. J. Johnston, *High-Lift Aerodynamics of Uninhabited Combat Air Vehicle Configurations with Reduced Radar Cross-Section Characteristics*, in *RAES Applied Aerodynamics Conference*, July 2012: Bristol.
- [19] J. Coppin, *Aerodynamics, Stability and Shape Optimisation of Unmanned Combat Air Vehicles*, in *Department of Mechanical Engineering*, 2014, University of Sheffield.
- [20] G. Lachmann, *Results of Experiments with Slotted Wings*, 1924, NACA.
- [21] H. K. Versteeg, and W. Malalasekera, *An Introduction to Computational Fluid Dynamics: The Finite Volume Method*, 2007, London: Pearson Education Limited.
- [22] C. B. Moler, *Numerical computing with MATLAB*, 2004: SIAM.
- [23] A. Ravindran, G. V. Reklaitis, and K. M. Ragsdell, *Engineering optimization: methods and applications*, 2006: John Wiley & Sons.
- [24] M. El-Sayed, T. Sun, and J. Berry, Shape optimization with computational fluid dynamics, *Advances in Engineering Software*, **36**(9): p. 607-613, 2005.
- [25] C. Linares, C. P. Lawson, and H. Smith, Multidisciplinary optimisation framework for minimum rotorcraft fuel and air pollutants at mission level, *The Aeronautical Journal*, **117**(1193): p. 749-767, 2013, 1968.
- [26] S. C. Chapra, and R.P. Canale, *Numerical methods for engineers : with personal computer applications*, 1985, New York: McGraw-Hill.
- [27] J. D. Anderson, *Fundamentals of Aerodynamics*, 2010, Boston: McGraw-Hill Education.
- [28] N. C. Lambourne, and D.W. Bryer, *The Bursting of Leading-edge Vortices: Some Observations and Discussion of the Phenomenon*, 1961.
- [29] C. Breitsamter, Unsteady flow phenomena associated with leading-edge vortices, *Progress in Aerospace Sciences*, **44**(1): p. 48-65, 2008.
- [30] P. B. Earnshaw, *An experimental investigation of the structure of a leading-edge vortex*, M.o. Aviation, Editor, 1961.
- [31] M. M. Yavuz, Transformation of flow structure on a delta wing of moderate sweep angle during pitch-up maneuver, *Journal of Fluids and Structures*, **33**: p. 59-69, 2012.
- [32] R. W. Johnson, *The handbook of fluid dynamics*, 1998, Heidelberg: Springer-Verlag.